**Fachtagung “Experimentelle Strömungsmechanik”**
7.–9. September 2021, Bremen

# PIV-LIF Untersuchungen von passivem Skalartransport über Bodenrippeln

## PIV-LIF Investigations of passive scalar transport above rippled seabeds

**L.Kandler[1], S. Grundmann[1], M. Brede[1]**
[1]Universität Rostock, Lehrstuhl Strömungsmechanik, Albert-Einstein-Str. 2, 18059 Rostock

PIV-LIF, Oszillierende Strömung, Rippel, Vermischung, Transport
PIV-LIF, oscillating flows, ripples, mixing, transport

### Abstract

The sediment-water interface of shallow coastal zones is an important gateway for terrestrial matter as well as for sediment originated (reaction) products. The discharge of pore- or groundwater is assumed to be mainly affected by wave driven flow regimes interacting with topographical features as sand ripples. Whereas wave-ripple interaction has been addressed by several studies, its influence on transport and mixing of discharging groundwater yet remains unrevealed. To foster the understanding of this aspect, the transport processes induced by wave-ripple interaction were reproduced and investigated in a lab experiment via synchronized PIV-LIF-measurements. For this purpose, a permeable seabed model with an idealised ripple structure was installed in a wave tank and perfused with a fluorescent tracer fluid. Particle Image Velocimetry (PIV) and Laser-Induced Fluorescence (LIF) were used to simultaneously measure velocity fields of the oscillating flow and spatial distributions of the discharging tracer fluid. Mixing and transport were characterised by post-processing and correlation of the phase averaged velocity and concentration data. It was found, that the different wave intensities and the resulting flow separation significantly affect the distribution and the mixing of the discharging fluid. Comparative measurements with a flat permeable bed showed, that the bottom topography is a second decisive influencing factor. The results led to the conclusion that the ripple topography causes much higher local tracer concentrations than flat seabeds whereas stronger wave intensities enhance the removal of tracer from the bottom boundary layer due to turbulent mixing and therefore lower local concentration values.

### Introduction

Sandy sediments cover more than 40% of the global inner continental shelf areas (Hall 2002). The high permeability of these sediments allows high flow rates through the sediment-water interface. This process facilitates the filtering of ocean water through the sediment as well as the transport of biogeochemical components and metabolic products of benthic organisms to overlying water layers (Huettel et al. 2014). Moreover, in case of submarine groundwater discharge (SGD), the sediment-water interface equals a terrestrial-marine gateway and allows the discharge of solutes as nutrients, carbon, metals or other materials (Taniguchi et al. 2019). In both cases, the discharging fluid affects benthic ecosystems and biogeochemical processes.

Wave induced flows and their interaction with the local seabed topography are among the major drivers of this interfacial fluid exchange (Santos et al. 2011). In case of sandy sediments, ripples are a common topographical seabed characteristic. Therefore, the transport and mixing of discharging fluid above permeable rippled beds are of great interest.

Huettel et al. 1996 experimentally investigated interfacial water flows in permeable sediments using a recirculating water tank. They observed the intrusion of a fluorescent tracer solute at small sand mounds and measured an increased pressure up- and downstream of these mounds under unidirectional flow conditions. Additionally, they observed a pressure drop at the downstream slope causing an advective transport of water from deeper sediment layers. Besides, the study addressed the intrusion of sand ripples. They found, that the ripple topography significantly increased the interfacial particle flux compared to a flat sediment bed. Precht et al. 2004 looked at the advective pore water exchange under oscillating flow conditions in a wave tank experiment. They focused on wave-ripple interactions as a main driver and influencing factor for pore water exchange within sandy sediments. In case of stationary ripples, they observed an intrusion at the ripple troughs and an upwelling of water from deeper sediment layers at the ripple crests. For beds with no significant topography only little transport could be observed, which was ascribed to small-scale advection, shear driven Brinkmann flow and molecular diffusion. Both studies mainly address transport processes within the sediment and do not consider the fluid dynamical processes above the sediment-water interface. However, Hare et al. 2014 measured three component flow velocities above sand ripples in a sinusoidal oscillating flow using a Doppler profiler. Yuan and Wang 2019 used PIV to obtain 2D velocity fields above sand ripples under acceleration skewed oscillating flow conditions. Both studies focus on wave-ripple interaction and describe downstream vortex formation behind the ripple crest. They also emphasized flow acceleration up the upstream side of the ripple and deceleration down the downstream side, which corresponds to the pressure drop described by Huettel et al. 1996.

Karow 2019 investigated transport and mixing of discharging groundwater in a similar experiment as in the study presented in this contribution and found dependencies on the wave intensity as well as the permeability and the slope angle of the seabed. However, he did not investigate rippled seabeds.

While no study addressing the transport and mixing of discharging water over sand ripples could be found, there are several studies investigating sediment transport within the boundary layer. Malarkey et al. 2015 measured velocity and sediment concentration fields above sand ripples in an oscillatory flow tank using a combination of PIV and an acoustic backscatter sensor. They also describe the formation of a downstream vortex at the ripple crest and its advection by the flow and underline the relevance of this vortex regarding mixing efficiency.

Although these studies might be an important component for understanding transport and mixing of discharging pore- or groundwater, more specialized investigations are essential to deepen the understanding of these processes. Therefore, a wave tank experiment using simulations PIV and LIF measurements to capture velocity and concentration fields has been established.

## Methods

Particle Image Velocimetry (PIV) is an optical measurement method for velocity field detection. Velocity vectors are detected based on the shift of tracer particles during a defined time interval. For this purpose, reflecting particles are added to the examined flow and exposed to a double laser light pulse while passing a laser light sheet defining the measurement area. The scattered light is detected by a charge-coupled device (CCD) camera with high spatial resolution. In the post processing, the resulting 2D-pictures are separated into interrogation areas. The shift vector of each interrogation area is defined by cross correlation functions. The spatial shift and the time interval between the laser pulses give the velocity vector for each interrogation area. (Raffel et al. 2018)
Laser induced fluorescence (LIF) is a method for concentration field measurements based on fluorescent light emission detection. The local fluorescence intensity of a tracer is proportional to its local concentration. The proportionality factor can be defined by a calibration curve. Hence, the intensity (brightness) of each pixel can be assigned to a specific concentration value. For the combination of PIV and LIF, the measurement setup includes two cameras, which simultaneously capture the same image section. (Crimaldi 2008)

## Experimental Setup

The experiments discussed in this contribution were conducted in a flow tank located at the chair of Fluid Mechanics at the University of Rostock, which has been adapted by Karow 2019 to facilitate oscillating flows. The tank (4.0 m long, 0.8 m wide and 1.0 m deep) consists of three major components: a wave generator at the one end of the tank, a flow section and a wave absorber at the other end of the tank as shown in the right part of Figure 1. The piston-type wave generator is composed of a vertical steel plate moving perpendicular to the longitudinal axis of the tank. The movement is driven by a motorised isel® toothed belt feed and controlled via the software proNC. The measurement section is located downstream of a settling section and contains a slot for an artificial seabed model (SBM). The panel wave absorber was installed to minimize wave reflection. It consists of ten steel panels, which are oriented perpendicular to the wave direction and are increasing in height towards the back wall of the tank (see also Karow et al. 2017).

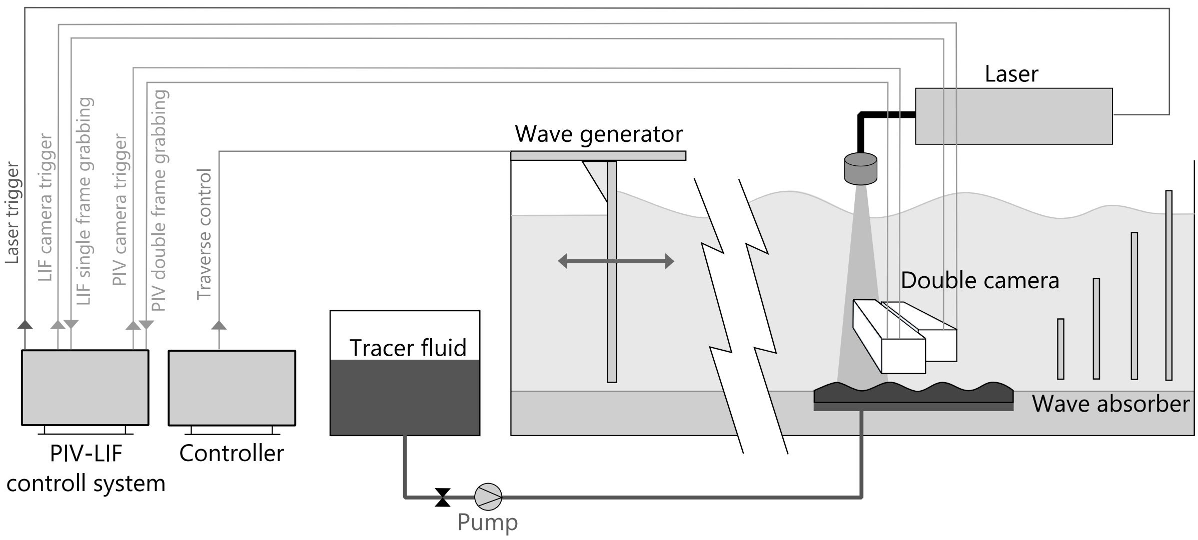


**Figure 1:** Experimental Setup including the wave tank (depicted on the right) and the PIV-LIF-system (depicted on the left)


GALA e.V., Karlsruhe, Germany, ISBN 978-3-9816764-7-1

Additionally to the wave tank, the experimental setup contains a tracer supply unit and a PIV-LIF measurement system as visualized in the left half of Figure 1. The tracer supply unit is designed to inject a fluorescent tracer fluid (FTF) into the wave tank to mimic groundwater discharge. It consists of a 5 l FTF storage tank, a submersible pump as well as a supply tube and a small reservoir underneath the SBM. In this study, the fluorescent dye Rhodamin 6G (Sigma-Aldrich®) with an absorption wavelength of 525-530 nm and an emission wavelength 590 nm (Yarborough 1974) was used. The submersible pump conveys the FTF into the tank. The inflow section for the FTF is placed at the bottom of the slot that contains the SBM. A dispersion device diffuses the fluid before it enters a gap underneath the SBM. Thus, a nearly pressure-free FTF reservoir is provided to facilitate a steady and homogenous perfusion of the permeable SBM. The PIV-LIF measurement system for simultaneous measurements of instantaneous velocity and concentration fields is composed of two CCD cameras, a laser light source and a control unit (computer) for measurement execution. The two Dantec Flowsense 2M cameras have a resolution of 1600 x 1200 pixels, a pixel size of 7.4 µm and a double frame rate of 15 Hz. They can be positioned via a triaxial traverse system. The field of view of the LIF camera, which has to be perfectly congruent with the field of view of the PIV camera, can be adjusted via a semi-reflective mirror. The mirror can be tilted into different directions via three adjusting screws. The PIV particles and the FTF are illuminated by a Litron Nd:YAG Laser with a wave length of 532nm. An optical light guiding arm deflects the laser beam first, onto a focus lens and second, onto a cylindrical lens, which creates the laser light sheet. The light sheet is aligned parallel to the longitudinal walls of the wave tank and guided into the water body through an acrylic Plexiglas® block. Data acquisition and triggering of the cameras and laser shutter were performed using the software Dantec DynamicStudio.

Three measurement configurations were performed using two different wave scenarios (“calm” and “stormy”) and two different SBM (flat and sinusoidal rippled): 1. Flat bed, calm wave Scenario 2. Rippled bed, calm wave scenario and 3. Rippled bed, stormy wave scenario. The wave scenarios were controlled via the feed, velocity and acceleration of the wave generator.
15 l of the fluorescent tracer were pumped into the reservoir during a PIV-LIF-measurement of 10.000 time steps. The post processing of the raw PIV- and LIF-data was done using DynamicStudio. Time resolved velocity vector and concentration fields were extracted and subsequently phase averaged. Velocity fluctuations were calculated to obtain phase averaged fields of turbulent kinetic energy.

## Results

Phase averaged measurement results of the three different experimental configurations are visualized in Figure 2. The upper graphs show the respective oscillating phase averaged mean velocity within the top level of the field of view for each configuration. The positions of three specific wave phase angles within the entire wave period are marked as “a”, “b” and “c”. Phase angle “a” corresponds to the point of maximum upstream velocity, phase angle “b” tags the wave’s turning point and phase angle “c” corresponds to the point of maximum downstream velocity. The plots below the upper row show the velocity and the concentration fields according to these phase angles for the three configurations respectively. The configurations are characterised by either a flat or a sinusoidal rippled SBM and a “calm” or “stormy” wave scenario. Highest local concentration values occur in case of the calm wave scenario and the rippled SBM directly within the bottom boundary layer. This highly concentrated layer is thicker in case of phase angles “a” and “c”, when maximum velocities occur. In contrast to the measurements with the calm wave scenario, the results for the stormy wave scenario show a cloud of higher tracer concentration emerging at the ripple crest and following the present main flow direction. The concentration field of this configuration thus shows a stronger dependency on the flow oscillation. Figure 3a depicts the mean phase averaged concentration profile of a whole wave period. The height of the field of view is normalized with the mean water depth $\overline{H(x)}$ to provide comparability between the measurement with a flat and those with a rippled bed. In case of the calm wave scenarios, much higher concentration values occur near the bed. However, in higher levels of the measurement area (from about 1.8 mm on), the concentration related to the stormy wave scenario and the rippled bed exceeds the concentration related to the calm wave scenario and the flat bed.

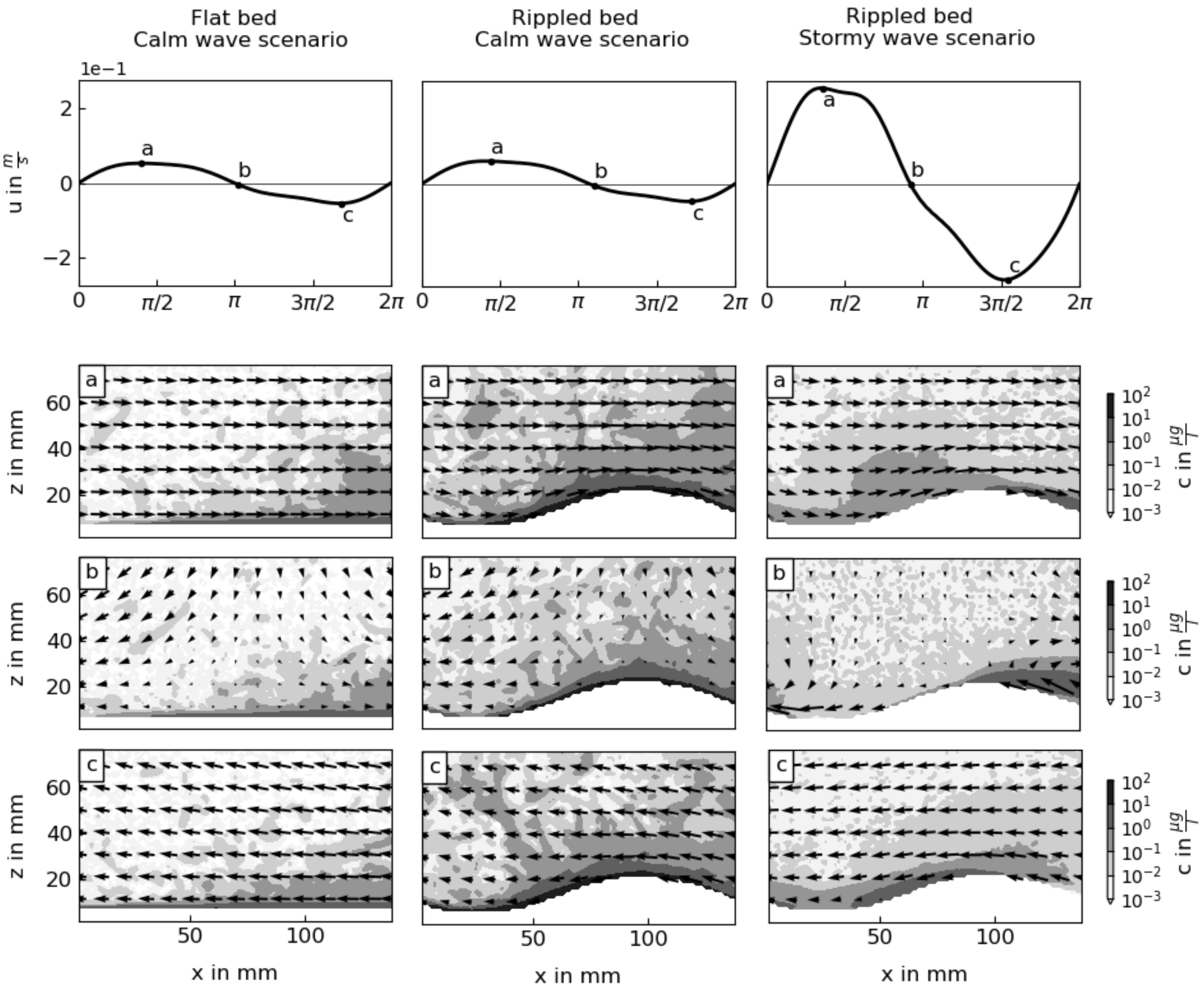


**Figure 2:** Phase averaged velocity vector and concentration fields for three different experimental configurations (columns) and three different wave phase angles (rows). The upper row shows the wave profile, respectively, and the position of the wave phase angles “a”, “b” and “c” related to the whole wave period

Figure 3b depicts the mean phase averaged profiles of turbulent kinetic energy (TKE). For both configurations with a rippled bed, TKE clearly increases towards the bottom of the tank. The configuration with the rippled bed and the stormy wave scenario shows the highest overall values for TKE. Therefore, Figure 4 visualizes the phase specific TKE fields of this measurement configuration. The highest local values for TKE occur in the case of maximum flow velocities and are located near the bed at the slopes of the ripple, while simultaneously the ambient flow is rather laminar. Furthermore, high local TKE can be found at the upstream side of the ripple slope while the top-level velocity is near its zero-crossings and thus, the wave changes direction. The last plot in Figure 4 (bottom right, VI) shows a recirculation bubble corresponding to the area of high TKE.

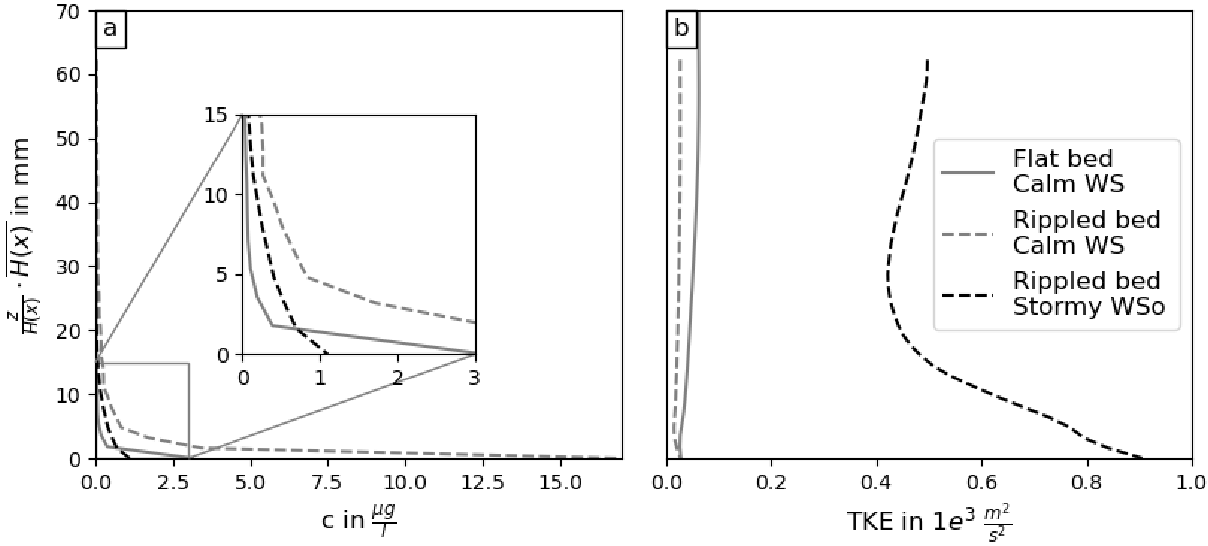


**Figure 3:** a) Mean phase averaged profiles of tracer concentration b) Mean phase averaged profiles of turbulent kinetic energy for different bottom topography and wave scenarios (WS)

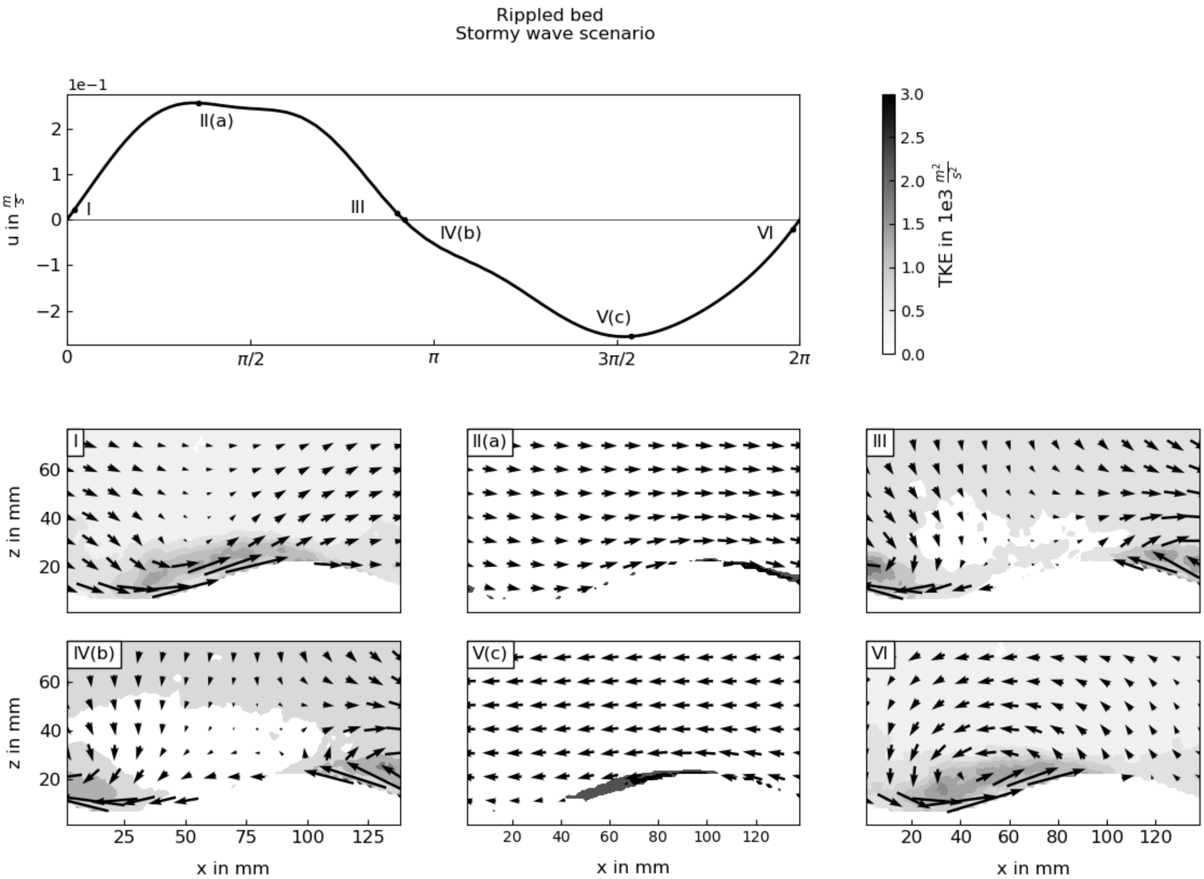


**Figure 4:** Phase averaged fields of velocity and turbulent kinetic energy for the configuration with rippled bed and stormy wave scenario corresponding to six different wave phase angles. The upper graph illustrates the wave profile and the position of the wave phase angles “I” to “VI” related to the entire wave period

## Discussion and Conclusion

Although the discharged volume flux of tracer fluid was equal for all three configurations, there are significant differences regarding the concentration values and the spatial distribution within the field of view. As clearly visible in Figure 2, in case of the calm wave scenario, the rippled bed results in a much higher tracer concentration within the boundary layer and hence leads to a stronger vertical transport through the permeable bed as compared to the flat bed configuration. This is due to acceleration of the flow at the ripple slopes, which causes a pressure drop near the crest and thus suction and upwelling of tracer fluid through the permeable bed, as already observed by Precht et al. 2004. Additionally, the mixing of the tracer is enhanced by the exchange between the boundary layer and the periodically agitated wake of the ripples.

Both effects are increased by higher flow velocities in case of the stormy wave scenario, while on the other hand the presence of more intense turbulence enhances the removal of discharging fluid due to turbulent transport and mixing and thus lowers the tracer concentration within the bottom boundary layer. However, the aspect of vortex formation and turbulent transport has to be further investigated in future studies. Turbulent flux as a parameter to quantify turbulent transport will be presented in the oral presentation. Besides, the aspect of intrusion and recirculation of tracer fluid within the permeable SBM has to be examined further. Additionally, the effect of more naturally shaped as well as asymmetric ripple profiles will be addressed in future experiments.

## Literature


**Crimaldi, J.P., 2008**: “Planar laser induced fluorescence in aqueous flows”, Exp Fluids 44, 6, 851–863.

**Hall, S.J., 2002**: "The Continental shelf benthic ecosystem: current status, agents for change and future prospects", Environmental Conservation 29 (3):350-374

**Hare, J. et al., 2014**: “Observations of the space-time structure of flow, turbulence, and stress over orbital-scale ripples”, Geophys. Res. Oceans, 119, 1876–1898

**Huettel, M. et al., 1996**: “Flow-induced uptake of particulate matter in permeable sediments”, Limnol. Oceanogr., 41(2), 309-322

**Huettel, M. et al., 2014**: "Benthic Exchange and Biogeochemical Cycling in Permeable Sediments", Annu. Rev. Mar. Sci. 2014. 6:23–51

**Karow, N. et al., 2017:** „Grundwassereintrags in marinen Bodengrenzschichten“, Experimentelle Strömungsmechanik, 25. Fachtagung, 5.-7. September 2017, Karlsruhe, Karlsruhe, Deutsche Gesellschaft für Laser-Anemometrie GALA e.V pp. 551–558

**Karow, N., 2019**: “Waves and turbulence on wavy coastal seabeds inducing vertical scalar transport”, Dissertation, University of Rostock

**Malarkey, J. et al., 2015**: “Mixing efficiency of sediment and momentum above rippled beds under oscillatory flows” Continental Shelf Research 108, 76–88

**Precht et al. 2004**: “Oxygen dynamics in permeable sediments with wave-driven pore water exchange”, Limnol. Oceanogr., 49(3), 693-705

**Raffel, M. et al.; 2018**: “Particle Image Velocimetry. A Practical Guide”, Springer International Publishing; Imprint; Springer, Cham

**Santos, I.R. et al., 2011**: “The driving forces of porewater and groundwater flow in permeable coastal sediments: A review” J.Wind Eng. Ind. Aerodyn. 49:351–368

**Taniguchi, M. et al., 2019**: "Submarine Groundwater Discharge: Updates on Its Measurement Techniques, Geophysical Drivers, Magnitudes, and Effects”, Front. Environ. Sci. 7:141

**Yarborough, J.M., 1974**: “cw dye laser emission spanning the visible spectrum”, Appl. Phys. Lett. 24, 12, 629–630.

**Yuan, J. and Wang, D., 2019**: “An Experimental Investigation of Acceleration-Skewed Oscillatory Flow over Vortex Ripples”, Geophys. Res. Oceans, 124, 9620–9643